Effect of Filler Particle Size on the Properties of Model Nanocomposites

D. Brown,*,† V. Marcadon,‡,§ P. Mélé,† and N. D. Albérola†

Laboratoire des Matériaux Organiques à Propriétés Spécifiques (LMOPS), UMR 5041 Université de Savoie−CNRS, Campus Scientifique, 73376 Le Bourget-du-Lac, France, and Laboratoire de Mécanique des Solides (LMS), UMR 7649 CNRS, Ecole Polytechnique, 91128 Palaiseau, France

Received August 28, 2007; Revised Manuscript Received November 13, 2007

ABSTRACT: Molecular dynamics simulations have been used to examine the effect of the size of a spherical inclusion in generic model polymer nanocomposite systems. Results are presented concerning the effect of the increasing particle size on the thickness of the interphase, i.e., the perturbed zone of polymer surrounding the inclusion. The behavior of the mass density, molecular orientation, fraction of *trans* conformers, as well as dynamic properties are presented as a function of the distance from the nanoparticle surface. The effect of temperature on these distributions is also discussed. Long simulations have been carried out to determine the variation in the glass transition of the filled polymers as compared to the pure systems. It is established that, within errors, the interphase thickness is independent of the size of the nanoparticle for the range of particle sizes analyzed. This information is particularly important for the second stage of the project where it is used in continuum micromechanical calculations to try to explain the behavior of the mechanical properties of the model nanocomposites. The confrontation between continuum and atomistic approaches will be the subject of a future publication.

1. Introduction

In a previous paper,[1] the results of a pilot study were presented of a molecular dynamics (MD) simulation of a model polymer nanocomposite system. This study explained in detail the motivation behind such studies and introduced a technique whereby a nanoparticle could be incorporated into a relaxed amorphous long-chain polymer system. Moreover, it proved the feasibility of obtaining statistically meaningful results for the variation of the structure and dynamics of the polymer chains as a function of the distance from the interface. Simulations at different pressures gave rise to the rather unexpected result that polymers filled with nanoparticles, dispersed in a perfectly ordered manner, could have *lower* bulk moduli than the pure polymer. Indeed, mainstream thinking in this respect claims that the reduced mobility of the polymer chains in the vicinity of the nanoparticle, as observed in experiments[2−5] and our and other MD simulations,[1,6−11] should lead to an interphase with *increased* mechanical properties. Thus the effect of reducing nanoparticle size, at constant volume fraction of filler, should be an (important) increase in the elastic moduli of the composite system as the volume fraction of interphase becomes important, i.e., at very small particle sizes. In reality, obtaining a perfect dispersion of nanoparticles in a polymer matrix is not straightforward. For a given volume fraction of submicronic inclusions, the distances between inclusions in the polymer matrix diminish drastically increasing the probability of the formation of aggregates and leading generally to a separation of the phases into independent connectivities or a cocontinuous phase.[12,13] This problem renders an experimental verification of the MD prediction for perfectly dispersed systems rather difficult but perhaps not beyond the realms of advances in preparation techniques. It is thus interesting to pursue the simulation approach in order to see whether this was a spurious result, although it has been seen in other systems by us[14] and by other authors,[15] or whether small particles indeed tend to act as plastifying agents which, although clearly leading to partial immobilization of chains at the interface, disrupt the packing of the polymer chains sufficiently to ultimately give an interphase with a mean density of the polymer lower than that of the pure bulk phase. To investigate this, we study here systems where the size of the inclusion is systematically increased. Our primary aim in this paper is first to establish, for the method of preparation employed,[1] what the dependence of the interphase thickness is on the size of the included particle. It is important here to make a distinction between cases where the polymer chains are in equilibrium with an interface, for which there are good reasons to expect a complete independence of interphase thickness on particle size,[16] and, as in here and in real composites, where the polymer is generally not in equilibrium with the filler due to the method of fabrication and the long relaxation times of the chains.

We emphasize that the simplified models developed in this study are not designed to represent any specific real system. They are specifically intended to be used to provide virtual data for mechanical properties against which continuum-based elastic micromechanical models will be compared. These comparisons will be the subject of a second paper.

2. Details of the simulations

2.1. The Silica Model. In our pilot study of a silica containing nanocomposite,[1] the silica was modeled using the potential of Tsuneyuki,[17] which was originally developed to represent the crystalline polymorphs of SiO_2. Although this model is relatively straightforward, containing just two-body Buckingham and Coulombic interactions for the partially charged Si and O atoms, the Ewald summation method,[18] which is used to take into account the Coulombic interactions, requires a significant amount of CPU time to achieve full convergence. As the specific nature of the

* To whom correspondence should be addressed. E-mail: David.Brown@univ-savoie.fr.

† UMR 5041 Université de Savoie−CNRS.

‡ Ecole Polytechnique.

§ Current address: ONERA−DMMP, Centre de Chatillon, BP 72, 29 avenue de la Division Leclerc, 92322 Chatillon, France.

10.1021/ma701940j CCC: $40.75
Published on Web 01/25/2008

Table 1. The Buckingham Potential (Eq 1) Parameters for the BKS Model of Silica

atom type 1	atom type 2	*A*/eV	*B*/Å	*C*/eV Å^6
Si	O	18003	0.205204	133.54
O	O	1389	0.362319	175.00

components of the composite is not relevant to this study, we simply require a hard isotropically elastic particle embedded in an isotropic softer medium, a much simpler model of a nanoparticle has been used in this work. Effectively, we take a sample configuration of the bulk amorphous SiO_2, generated using standard two-body potentials, and then introduce explicit Si−O bonds to form a network structure. By then adjusting the strengths of the Si−O bonds and the stiffness of the O−Si−O and Si−O−Si valence angle potentials, it is possible using these "intramolecular" potentials alone to maintain a rigid structure with approximately the same radial distribution functions and, importantly, having about the same elastic moduli of the bulk "atomic" model. The substitution of the two-body Van der Waals and Coulombic potentials by a small number of near-neighbor bonds and angles of course reduces enormously the computing time required and thus renders much more accessible systems with larger particles. By maintaining an atomic structure for the particle, rather than simply using a large sphere,[6,7] it is possible to determine the elastic moduli of the pure "silica". This is particularly important regarding the second phase of the work where the elastic moduli of the pure silica and pure polymer phases are used as input to the continuum mechanics calculations. However, in terms of the results presented in this paper, the use of a simple sphere to model the nanoparticle is probably a valid alternative. It should also be noted that the use of intramolecular potentials alone minimizes the possibility of any size-dependent changes in the rigidity of the nanoparticle. In reality the convergence of the properties of small particles toward bulklike values must be governed by the effective range of the intermolecular forces. This is an interesting subject in itself but beyond the scope of this paper.

2.1.1. Atomistic Model. In this work, the starting point for the simulation of silica in the bulk phase is the BKS model of Van Beest, Kramer, and Van Santen.[19] This model is very similar to that of Tsuneyuki[17] in that SiO_2 is represented as point ions, with charges of $q_{Si} = 2.4$ e and $q_O = -1.2$ e, which interact through a combination of Coulombic forces and Van der Waals (VdW) terms. The main difference between the two models is the absence of a VdW potential for the Si···Si interactions in the BKS model; these are considered unnecessary given the large positive charges on the ions. In the BKS (or Tsuneyuki) model, the VdW terms are parametrized using the Buckingham (exponential-6) form

$$\Phi_{\text{Buck}}(|\mathbf{r}_{ij}|) = A \exp(-|\mathbf{r}_{ij}|/B) - C|\mathbf{r}_{ij}|^{-6} \quad (1)$$

The parameters in the BKS case are given in Table 1. An additional consideration for our choice of potential is that we wish to prepare the silica in an amorphous form and as this has already been successfully done with the BKS model.[20]

The starting structure for the MD simulation was the crystal structure of α quartz. A system of 1125 atoms, i.e., a supercell of $5 \times 5 \times 5$ unit cells, was first equilibrated at 300 K at a pressure of 1 bar for a period of 200 ps. This MD simulation was performed using the *gmq* MD program[21] running on an SGi O2 workstation. As the sole purpose of this simulation was to generate an amorphous silica-like structure, a fairly large time step of 5 fs was used. Each time step took about 0.92 s of CPU time. The average temperature was kept close to 300 K using the loose-coupling method of Berendsen et al.[22] with a τ_T of 0.1 ps. The average on- and off-diagonal components of the pressure tensor, **P**, were maintained close to their required values of 1 bar and zero, respectively, using a loose-coupling method[23] with a τ_P of 10 ps.[21] We refer subsequently in the text to this type of simulation in which the number of atoms is constant and the temperature and pressure tensors are controlled using loose-coupling techniques as "NPT" conditions. The truncation radius for Buckingham and for the real-space part of the electrostatic potential interactions, R_c, was set throughout at half the minimum perpendicular distance between any two opposite faces of the periodic MD box and thus varied with time. Long-range corrections to the energy and the pressure were made on the assumption that $g(r) = 1$ beyond the cutoff. Optimum convergence of the Ewald sum[18] was obtained by using a separation parameter $\alpha = 0.36$ Å^{-1} and a reciprocal space cutoff $K_{max} = 12$.[21] These values give convergence of the direct and indirect routes to the reciprocal space part of the Ewald sum contribution to the pressure of better than 10 bar.[24]

To obtain an amorphous sample of silica, the temperature was increased in the simulation to 10 000 K while maintaining the pressure at 1 bar. Once equilibrated in the molten state, the simulation cell was orthogonalized and the cell lengths equalized in order to obtain (momentarily) a cubic box. The system was then cooled down to 100 K at a rate of −100 K ps^{-1}, in a similar manner to that employed by Vollmayr.[20] Again pressure coupling was employed, and the box was allowed to change shape and size in response to the differences between the measured and required pressure tensors. The silica remaining amorphous at such high rates of cooling the MD cell stayed close to cubic with a side length of ∼25 Å once relaxed at 100 K.

From this 1125-atom system, a much larger sample was created by replicating the system three times in each direction. This led to a system containing $27 \times 1125 = 30375$ atoms with a side length of ∼75 Å. To decorrelate the system, the velocities of all the atoms were randomized and then equilibrium simulations were performed under NPT conditions at 1000 K for 40 ps. The parameters for the Ewald summation were retuned and optimum convergence was found using $\alpha = 0.29$ Å^{-1} and $K_{max} = 20$. The system was then cooled back down to 100 K.

2.1.2. Simplified Molecular Model. The 1125-atom system created using the BKS potential served as the basis for the parametrization of the "molecular" model of silica, as explained above. The pure bulk amorphous SiO_2 configuration equilibrated at 100 K was scanned and all Si and O atoms having a nearest-image distance less than 1.9 Å, i.e., one that encompasses the first peak in the Si···O radial distribution function, were deemed to be bonded. This operation effectively creates an infinite network of bonds. To maintain the structure close to the input configuration, the Si−O bonds defined are subject to a harmonic spring potential

$$\Phi_b(|\mathbf{r}_{ij}|) = (1/2)k_b(|\mathbf{r}_{ij}| - b_o)^2 \quad (2)$$

and a harmonic valence angle potential is used for all O−Si−O and Si−O−Si angles

$$\Phi_\theta(\theta) = (1/2)k_\theta(\cos\theta - \cos\theta_o)^2 \quad (3)$$

By trial and error it was found that the input distributions of the Si−O bond lengths and the O−Si−O and Si−O−Si angles could be reasonably maintained using for the Si−O bond $k_b = 800$ kg s^{-2} and $b_o = 1.6246$ Å, for the O−Si−O angle $k_\theta = 600$ kJ mol^{-1} and $\theta_o = 109.5°$, and for the Si−O−Si angle $k_\theta = 400$ kJ mol^{-1} and $\theta_o = 145°$.

Having optimized the parameters, they were then satisfactorily tested on the larger 30 375-atom system. This larger system was then equilibrated for 100 ps at 100 K and at the operating pressure of 5000 bar using a time step of 2 fs. As in our previous simulation,[1] nonbonded interactions between polymer atoms are completely repulsive in nature and thus a compensating overpressure is necessary to maintain a reasonable density for the polymer. The average density of the amorphous molecular SiO_2 model under these conditions was 2518.6 ± 0.1 kg m^{-3}.

As will be explained in a future article, the elastic moduli of this bulk SiO_2 model have been evaluated and have been found to be of the same order of magnitude as those of silica glass. In addition, the elastic moduli and Poisson's ratio have been checked for consistency against the formulas of isotropic linear elasticity. The agreement is reasonably good when taking into account the

error bars. This is an important consideration regarding the future comparisons with the continuum mechanics calculations.

2.1.3. Nanoparticle Preparation. The method used here to prepare a model silica-like nanoparticle is based on techniques previously used to prepare fairly realistic models which contained silanol groups on the surface.[14,25,26] In reality, silica generally contains a certain number of silanol groups (Si−O−H). Their exact number and location, surface or interior, depend on many parameters, and a number of experimental techniques exist which can be used to try and probe this.[27] The existence of silanol groups on the surface poses a number of problems as the BKS model has been developed to represent SiO_2 in the pure bulk state. However, other models have been used to represent essentially static surfaces of silica.[28−30] In order to resolve this problem, a hybrid model was developed[14] in which a modified BKS potential was used to represent the core of the nanoparticle while the surface was represented using a model for the surface of SiO_2.[28] With this completely dynamic model, the thickness and silanol coverage of the surface could be controlled while maintaining the structural characteristics of the interior in line with those for bulk amorphous silica. This model allowed us to mimic the surface of silica while keeping the structural characteristics of the core similar to bulk silica.

For the purpose of this study, there is no need to consider the silanol hydrogens, and the core atoms can be treated in the same way as the surface atoms model, i.e., as a network of Si−O bonds with the same force constants for the bonding and bending potentials as in the bulk molecular SiO_2 model. Nevertheless, for the purpose of constructing the nanoparticle, it is useful to maintain the artificial distinction of "surface" and "core". Thus, in the model, five different atom types are distinguished: the core silicon (Si) and oxygen (O) atoms, silicon atoms deemed to be in the surface layer (Si_s), oxygen atoms in the surface bridged between two surface silicons (O_b), and nonbridging oxygen atoms linked to only one silicon (O_nb). The problem then is to define which atoms are surface and which are core given a configuration of amorphous silica, a target radius for the nanoparticle, R_n, a definition of the radius of the core, r_n, and a definition of a maximum distance between silicon and oxygen atoms constituting near neighbors; as before this latter distance is taken to be 1.9 Å. To do this, we have implemented an algorithm similar to that used previously to define the surface of a cylindrical pore in silica.[28] The basic algorithm first removes atoms beyond the desired radius, R_n, and then discards all silicons in the surface layer having fewer than four near-neighbor oxygens. It then starts to build a connectivity table for the surface layer by first identifying those oxygens which are nonbridging, i.e., those with one near-neighbor silicon. This in turn identifies some of the surface silicons, i.e., the ones bonded to the nonbridging oxygens. There then follows an iterative procedure to propagate the connectivity of the surface layer by identifying the bridging and surface silicons successively. In detail, the algorithm is as follows.

Step 1: Read the previously prepared bulk configuration of amorphous SiO_2.

Step 2: Discard all atoms that lie further from the origin than the nominal radius, R_n, of the nanoparticle.

Step 3: For each silicon, identify, store, and count all the near-neighbor oxygens, i.e., those that lie within 1.9 Å.

Step 4: Eliminate all silicons in the surface layer, i.e., those further from the center than r_n, which have less than four oxygen neighbors.

Step 5: Eliminate all oxygens in the surface layer having no silicons within 1.9 Å.

Step 6: Identify all the nonbridging oxygens as those having just one silicon within a distance of 1.9 Å. Set the connectivity table for each atom to indicate a bond between them.

Step 7: Label all silicons with a nonbridging oxygen as a neighbor as being surface silicons.

Step 8: Visit all surface silicons and label all non nonbridging oxygens within 1.9 Å as being bridging oxygens. Update the respective connectivity tables to form bonds between the surface silicons and the bridging oxygens.

Step 9: Loop over all bridging oxygens and find all nonsurface silicons within 1.9 Å that are further from the center than r_n. Label these silicons as surface silicons and update the connectivity tables.

Step 10: If either the number of nonbridging oxygens added at Step 8 or the number of surface silicons added at Step 9 is nonzero go to Step 8.

Step 11: Visit all the bridging oxygens and check if they are bridged between two surface silicons. If not change the type of the atom back to a regular core oxygen BUT keep the connectivity table unchanged to indicate a bond between this oxygen and the surface silicon.

Step 12: Visit all core silicons and find all core oxygens within 1.9 Å. Update the respective connectivity tables to form bonds between the core silicons and oxygens.

This basic algorithm gives spherical particles with a certain surface roughness, depending on the initial configuration and the elimination of silicons not connected to four oxygens. To ensure that the atoms in the surface layer formed a percolating network, it has been found previously[14] by trial and error that r_n has to be defined to be about $R_n - 9$ Å. Thinner surface layers tend to lead to rather patchy surface networks or even nonpercolating ones.

By use of the above algorithm and the equilibrated BKS 30375-atom configuration at 100 K as input, nanoparticles with $R_n = 15$ Å and $R_n = 30$ Å were created directly, as the side length of the input cell was sufficiently large at ∼75 Å. To create an even larger particle with a radius of 60 Å, the 30375-atom configuration was scaled up by a factor of 2 in each direction and then used. No attempt was made to decorrelate the positions in this case as the surface in each quadrant results from a different way of cutting through the original system. The three nanoparticles were then relaxed at 100 K using the same bond and bond angle bending potential parameters of the molecular model of the bulk. They were then ready to be inserted into the polymer matrix to form the model nanocomposites.

2.2. The Model Polymer Matrix. 2.2.1. Preparation. As there are no longer nonbonded interactions in the silica model for the nanoparticle, there is no longer any need to use a Buckingham potential for the polymer, as in our previous work.[1] In this case, we can thus revert to using exactly the same model as the one which has been often employed to study amorphous polymer systems.[31−34] In this model, linear chains of n united-atom CH_2 sites are held together by rigid bonds and valence angle and torsion angle potentials give internal structure and rotational barriers. Nonbonded interactions are represented by a purely repulsive potential that operates for all intermolecular pair interactions and between all pairs of sites in the same chain separated by at least three intervening ones. This potential takes the form of a Lennard-Jones (LJ) 12−6 potential truncated at the minimum and raised up by the well depth to give a repulsive potential smoothly decaying to zero, often referred to as a Weeks−Chandler−Andersen, or WCA, potential

$$\Phi_{WCA}(|\mathbf{r}_{ij}|) = 4\epsilon((\sigma/|\mathbf{r}_{ij}|)^{12} - (\sigma/|\mathbf{r}_{ij}|)^{6}) + \epsilon \quad \text{for } |\mathbf{r}_{ij}| \le 2^{1/6}\sigma \tag{4a}$$

$$\Phi_{WCA}(|\mathbf{r}_{ij}|) = 0 \quad \text{for } |\mathbf{r}_{ij}| > 2^{1/6}\sigma \tag{4b}$$

The parameters are taken as $\epsilon/k_B = 57$ K and $\sigma = 4.28$ Å in the case of these united-atom CH_2 sites. As before, to compensate for the lack of an attractive part to the potential, a hydrostatic overpressure of 5000 bar is applied.

For the purpose of this study, four systems were prepared with 10, 30, 80, and 640 chains of $n = 1000$ CH_2 sites per chain. The 30-chain system was used simply to study the pure matrix and not as the basis of a composite system. A generation technique,[33] known to produce representative configurations from the dense amorphous phase,[34] was used to set up the systems. We note in passing that this technique has since been generalized to arbitrary linear polymers[35] and is now a robust method which has been tested and validated on diverse polymers.[36] The method, as used here, consists of an initial single-chain sampling phase of an isolated chain subject to pivot Monte Carlo moves for bond angles and dihedral angles

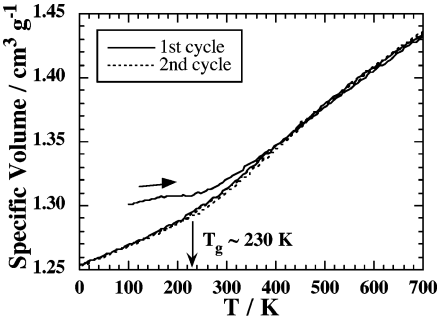

Figure 1. The specific volume plotted as a function of the temperature for the two heating and cooling cycles performed on the 30 000-atom pure matrix system. Note that the path taken during the first heating differs from the rest.

in which nonbonded interactions are restricted to just those atoms separated by three others along the chain; all other nonbonded interactions are ignored. The configurations of the desired number of chains are taken from the resulting sequence, and each chain configuration is randomly reorientated and then randomly inserted into a standard periodic cubic MD cell of a size corresponding to an initial density of ~630 kg m^{-3}. This density represents a compromise between a density which is not too high as to give problems when the rest of the nonbonded interactions are introduced and the one which is not too low that the resulting isotropic compression leads to distortion of the carefully prepared chain conformations.

It is important to specify the temperature used during the single-chain sampling phase as this controls the initial configurational properties, e.g., the distribution of end-to-end distances of the chains, and as natural relaxation times of these chains are quite long, these initial distributions are changed little by the relaxation in the second phase.[34] This is exactly the principle exploited by the generation procedure. From previous work, it is known that the sampling temperature has an influence on the mechanical properties of the polymers,[37] particularly in the post-yield behavior. In this work, a fairly high sampling temperature of 500 K was used. This was to ensure that the chains were relatively well coiled and thus will minimize the possibility of sequences of *trans* conformers forming with the concurrent risks of crystalline domains developing. Our aim is to have a perfectly amorphous polymer matrix that shows isotropic elastic behavior. Partially crystalline samples would compromise the subsequent comparisons with the continuum mechanics calculations.

In a second stage, the nonbonded interactions, ignored in the first phase, are smoothly introduced into the resulting multi-chain configuration. The systems were then relaxed using MD at constant volume and loose-coupling controlled temperature conditions (NVT) for 100 ps at 100 K in order to allow the systems to come to thermal equilibrium. An annealing step was then carried out at 1000 K for 100 ps, while keeping the volume constant, to try to relax the system further. Afterward, it was relaxed again for 100 ps under NVT conditions at 100 K before being simulated for 2000 ps under NPT conditions at an isotropic pressure of 5000 bar. For these simulations, the time step was set to 2 fs, to take into account the higher frequency oscillations, and the loose-coupling constants used were $\tau_P = 2$ ps and $\tau_T = 1$ ps. Bond length constraints were satisfied to a relative tolerance of 10^{-6}. Characteristics of the four relaxed systems after this initial relaxation were very similar. The average density was about 767 kg m^{-3} with a spread between the different samples of about ± 1 kg m^{-3}. All samples gave mean percentages of 72.7 $\pm$ 0.1 of the *trans* conformers.

The configurations thus obtained for the 10-, 80-, and 640-chain systems served as the initial matrix configurations for the preparation of the composite systems. As the preparation and relaxation of the composite systems (see Section 2.3) involve an annealing step as well, it is important, for the comparisons that follow, to try and match the thermal history of the pure matrices to those of the matrices in the composites. For this reason, all systems were further relaxed for another 220 ps under NPT conditions at 100 K at an applied isotropic pressure of 5000 bar. There then followed a second 100 ps simulation under NVT conditions at 1000 K to anneal the system in the same way as that of the composites. After annealing, the temperature was returned to 100 K and a further 100 ps of NVT MD was performed in order to re-thermalize the systems at 100 K. Systems were then relaxed for another 2000 ps using NPT MD at 100 K and 5000 bar. Average properties for the pure matrices following this second heat treatment are given in Table 2.

Table 2. System Characteristics and Average Properties from the Simulations of the Pure Matrices at 100 K and a Pressure of 5000 Bar[a]

	pure matrices		
no. of chains	10	80	640
total no. atoms	10 000	80 000	640 000
C−C−C bend energy	494 ± 1	497 ± 1	499 ± 1
torsion energy	2097 ± 5	2085 ± 6	2076 ± 5
VdW energy			
$CH_2\cdots CH_2$ total	788 ± 1	786 ± 1	784 ± 1
$CH_2\cdots CH_2$ inter	614 ± 1	618 ± 1	613.0 ± 0.2
$CH_2\cdots CH_2$ intra	174 ± 1	168 ± 1	171.3 ± 0.5
density/kg m^{-3}	774.9 ± 0.2	776.6 ± 0.2	775.7 ± 0.1
% *trans*[b]	69.3 ± 0.1	69.6 ± 0.1	69.8 ± 0.1

[a] All averages were taken over the last 1500 ps of each simulation following the second heat treatment (see text for details). Average energies are quoted in J/mol of CH_2 Sites. [b] *% trans* is the mean percentage of *trans* conformers of the polymer chains.

2.2.2. Glass Transition. To ensure that the temperature of 100 K, chosen for the main part of the investigation of the mechanical properties of solid polymer composites, was below the glass transition temperature, T_g, separate heating and cooling cycle simulations were also performed. From the start of the final configuration of the relaxed 30-chain system at NPT 100K and 5000 bar, the temperature was linearly increased at a rate of 0.1 K ps^{-1} up to a temperature of 700 K. The system was then allowed to relax at 700 K under NPT conditions for 500 ps, and then the temperature was decreased at a rate of -0.1 K ps^{-1} down to 0 K. For comparison, a second cycle was carried out in a similar fashion.

The curve of specific volume ($V_{spec} = 1/\rho$) against temperature for these two cycles, Figure 1, shows that the first time the system is heated it follows a different path; otherwise the heating and cooling curves are quite close. This is very typical of polymer systems having been subject to different thermal histories. There is also a change in slope of the curves between 150 and 300 K. We first tried fitting straight lines to $V_{spec}(T)$ either side of T_g and then determining the intersection point, but this procedure does not use all the data and leads to results which are very sensitive to the exact range of temperatures chosen for the linear least-squares fits. For this reason, we tried to ascertain the glass transition temperature in a more objective manner by using least-square regression fits in the entire range from 0 to 450 K, i.e., about 200 K either side of T_g, using the following combination of two linear functions

$$V_{spec}(T) = (a + bT)(1 - S(T)) + (c + dT)\,S(T) \qquad (5)$$

where a, b, c, and d are constants and $S(T)$ is a switching function which goes from 1 to 0 in a controllable interval either side of T_g. In this work, the following form for $S(T)$ has been chosen

$$S(T) = \frac{1}{2}\left(1 + \frac{T - T_g}{\omega + |T - T_g|}\right) \qquad (6)$$

where ω is the parameter controlling the sharpness of the switching function; $\omega = 0$ being the standard Heaviside function. A value of $\omega = 1$ was used to fit the specific volume vs T curves, and from both the first and second cooling curves, a T_g of about 230 K was obtained from the best fits. It has to be stated with precaution though that the errors in T_g using this approach are inevitably quite important due to the rather subtle changes in the slope of $V_{spec}(T)$.

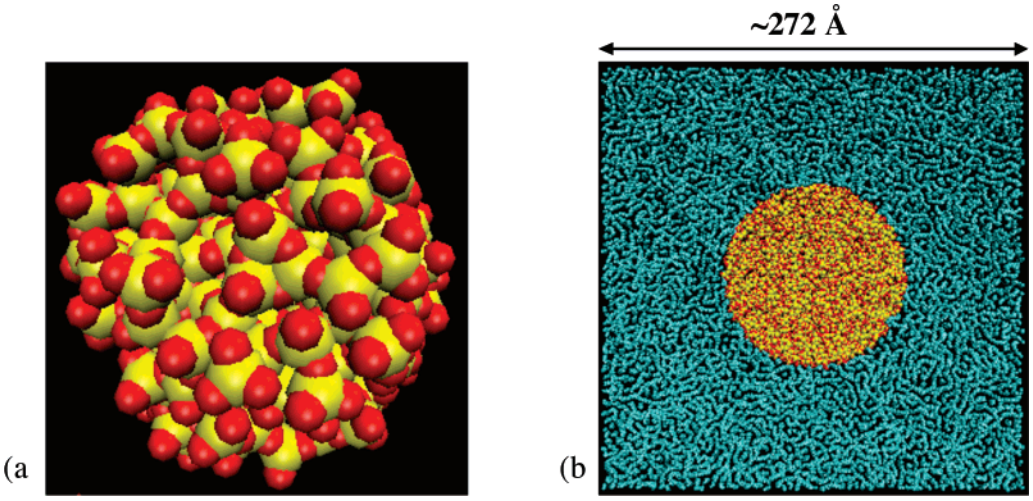

Figure 2. (a) A close-up 3D view of the $R_n = 15$ Å silica nanoparticle. (b) A thin cross-section through the center of the R60L composite system which contains a nanoparticle of silica with a radius of ~60 Å in a box of 640 chains of 1000 monomers per chain. The entire system contains 705181 atoms. In both pictures, oxygen atoms are shown in red and silicon atoms in yellow. In (b) CH_2 units are shown in light blue. Images were produced from the coordinates of the atoms using the VMD program.[38]

Nevertheless, at a temperature of 100 K, the model polymer matrix is well into the glassy state.

2.3. The Model Composites. 2.3.1. Assembly. The method used to introduce a silica particle into a polymer matrix has been described before in detail.[1] Essentially the box of polymer is first increased by a volume corresponding to the particle that is to be inserted. A spherical cavity is then generated by gradually introducing a repulsive potential at the center of the box. The radius of this cavity grows at a rate of 1 Å ps^{-1} during a standard MD NVT simulation until the desired size is attained. This creates a spherical space into which the silica particle can be inserted. To avoid too much initial overlap between the polymer and the particle, the cavity is created 2 Å larger than R_n. In the final stage, the repulsive potential is switched off and the system is allowed to relax. In this respect, it has been argued[1] that the method corresponds to one where the nanoparticles are considered as being mechanically mixed into an existing equilibrium melt of very high viscosity. There is thus little chance that the system can attain thermodynamic equilibrium in any reasonable time scale, as is frequently the case in reality.

When the particle is inserted into the cavity, the interactions between the atoms of the silica particle and the CH_2 sites have to be taken into account. As the nanoparticle preparation method leads to a surfeit of oxygens at the surface, only the interactions between the surface O atoms and CH_2 sites were considered necessary to prevent polymer infiltration. This limits the number of pair distances that have to be calculated at each time step thus increasing efficiency. The cross interaction term between the polymer and oxygen have been taken from our previous work on more realistic models[14,25] and are $\sigma = 3.09805$ Å and $\epsilon/k_B = 64.806$ K. These nonbonded interactions are again defined using the WCA potential, so are purely repulsive.

Three composite systems were prepared at a fairly low target volume fraction of silica of ~4.5% by combining the 10-chain polymer matrix with the $R_n = 15$ Å particle, the 80-chain system with the $R_n = 30$ Å particle, and the 640-chain system with the $R_n = 60$ Å particle. These systems are referred to henceforth as R15L, R30L and R60L, respectively. Two other systems at a much higher target volume fraction of ~27% silica were prepared by combining the $R_n = 30$ Å particle with the 10-chain polymer matrix (R30H) and the $R_n = 60$ Å particle with the 80-chain matrix (R60H). As is explained later, the actual measured volume fractions differ slightly from the target ones due to the way in which the surface of the nanoparticles are prepared.

2.3.2. Relaxation Procedure. To avoid as much as possible the effects of different thermal histories, care was taken to prepare all the nanocomposite systems in the same way. The following schedule was used in each case. After assembly, a 20 ps NVT simulation at 100 K was first carried out to allow the kinetic energy to come to equipartition. A 200 ps NPT simulation then followed at 100 K at an applied isotropic pressure of 5000 bar. This allows the box size and shape to adjust to the imposed conditions. There then followed a 100 ps simulation under NVT conditions at 1000 K to anneal the system. This was done with the intention of alleviating any local interaction hot spots introduced by the assembly and was not without consequences (see later). After annealing, the temperature was returned to 100 K and a further 100 ps of NVT MD was performed in order to re-thermalize the systems at 100 K. Systems were then relaxed for 2000 ps using NPT MD at 100 K and 5000 bar. The configurations obtained at the end of this relaxation procedure served as the basis for the various mechanical and thermal experiments subsequently undertaken. An illustration of the largest system simulated is given in Figure 2.

The characteristics of the different pure matrix and composite systems simulated at 100 K are given in Tables 2 and 3.

For the MD simulations of the composite systems, the time step was maintained at 2 fs and the loose-coupling constants used were $\tau_P = 2$ ps and $\tau_T = 1$ ps, as for the polymer alone.

2.3.3. Glass Transition. To determine whether the included particle had any influence on the glass transition of the polymer matrix, a single heating and cooling cycle was performed in exactly the same way as that for the 30-chain pure polymer matrix. The final configurations of the relaxed composite systems at NPT 100 K and 5000 bar were heated up to 700 K, allowed to relax at 700 K under NPT conditions for 500 ps, and then cooled down again at a rate of -0.1 K ps^{-1} to 0 K. On the basis of the results for the pure matrix, no second cycle was carried out, and the T_g was obtained from the cooling branch of the specific volume vs temperature curve using nonlinear least-squares regression fits to the form of eq 5. The values found are shown in Table 4.

The MD simulations described in this section were mostly carried out using the general purpose parallel MD program *ddgmq*[21,39,40] running on eight processors on various supercomputers at IDRIS (Orsay, France) and CINES (Montpellier, France). For the R60L system containing over 700 000 atoms, for example, it took about 60 h to simulate 1 ns on eight processors of an IBM Power 4 machine. The smaller systems required proportionately less time. Further simulations were carried out using the scalar version of the code, *gmq*, on SGi workstations and a COMPAQ DS20E biprocessor server.

Table 3. System Characteristics and Average Properties from the Simulations of Composite Systems at 100 K and a Pressure of 5000 Bar[a]

	R15L	R30L	R60L	R30H	R60H
no. of chains	10	80	640	10	80
no. of Si atoms	277	2482	21 154	2482	21 154
no. of O atoms	649	5374	44 027	5374	44 027
total no. atoms	10 926	87 856	705 181	17 856	145 181
mass fraction of SiO_2	0.1146	0.1218	0.1264	0.5260	0.5364
C−C−C bend energy	497 ± 1	500 ± 1	500 ± 1	509 ± 1	504 ± 1
torsion energy	2080 ± 10	2060 ± 10	2060 ± 10	2020 ± 20	1990 ± 20
VdW energy					
total	793 ± 1	788 ± 1	787 ± 1	814 ± 2	800 ± 2
inter	625 ± 1	622 ± 1	621 ± 1	655 ± 2	651 ± 2
$CH_2\cdots SiO_2$	13.5 ± 0.1	8.12 ± 0.02	4.32 ± 0.02	67.7 ± 0.4	35.4 ± 0.2
	0.011 ± 0.001	*0.0109 ± 0.0003*	*0.0109 ± 0.0005*	*0.0114 ± 0.0001*	*0.0111 ± 0.0001*
$CH_2\cdots CH_2$ total	780 ± 1	780 ± 1	783 ± 1	746 ± 2	764 ± 2
$CH_2\cdots CH_2$ intra	168 ± 1	167 ± 1	166 ± 1	161 ± 2	149 ± 2
density/kg m^{-3}	845.5 ± 0.1	848.9 ± 0.2	851.5 ± 0.2	1232.5 ± 0.3	1239.3 ± 0.4
% *trans*	70.1 ± 0.1	70.3 ± 0.1	70.2 ± 0.1	71.3 ± 0.1	71.8 ± 0.1

[a] Column headings indicate the nominal size of the included particles and the nominal volume fractions of silica, e.g., R15L implies an $R_n = 15$ Å particle in a polymer matrix at the lower volume fraction of silica. Average energies are given in J/mol of CH_2 sites except for the figures in italics that are the $CH_2\cdots SiO_2$ VdW energies divided by the effective surface areas, $4\pi R_0^2$ (see Section 3.2.1. for the definition of R_0), of the nanoparticles. These surface energies are quoted in J m^{-2}

Table 4. Glass Transition Temperatures for the 30-Chain Pure Matrix System and Different Composite Systems[a]

	pure matrix	R15L	R30L	R60L	R30H	R60H
specific vol						
first cool	230 ± 50	230 ± 40	230 ± 40	230 ± 20	210 ± 40	220 ± 15
second cool	230 ± 40					
enthalpy	233 ± 13	228 ± 16	236 ± 12	235 ± 21	231 ± 17	234 ± 16
torsion energy	234 ± 10	228 ± 12	236 ± 11	234 ± 19	234 ± 11	237 ± 15
VdW energy	238 ± 2	267 ± 5	253 ± 15	268 ± 18	287 ± 2	263 ± 12
% *trans*	239 ± 10	231 ± 10	250 ± 10	252 ± 8	223 ± 1	233 ± 8

[a] As explained in the text, different estimates of T_g were obtained from the behavior of the various properties indicated in the table during the cooling runs. The enthalpy was evaluated using the expression $H = U + PV$, where U is the internal energy, P is the pressure, and V is the volume of the system.

3. Results and Discussion

3.1. Thermodynamic Data. 3.1.1. Energies. The averages of various thermodynamic properties are given in Tables 2 and 3 for the simulations of the pure matrix and the composite systems at 100 K, respectively. Averages were taken over the last 1500 ps of each simulation. The total potential energy has been partially resolved into its component parts in Tables 2 and 3 in order to see the underlying variations. Energies are generally quoted in Joules per mole of CH_2 sites so as to have a common normalizing factor.

For the pure matrix systems, the results are fairly consistent between the different system sizes. There does not appear to be any systematic change with system size, and the slight differences are typical of the normal variations one obtains when preparing different, relatively small, samples using the same technique.[32,34,36] In the case of the composite systems, similar variations from sample to sample must also exist. However, it can be seen that, as we have found before,[1] the relatively stiff C−C−C bending mode is hardly affected. The introduction of the nanoparticles and the subsequent program of relaxation does, however, induce some slight changes in the torsional energies consistent with the higher percentages in the *trans* conformers. We discuss more about the reasons for this in the section concerning the fraction of *trans* conformers.

It is particularly noticeable in Table 3 that the $CH_2\cdots O$ VdW energy decreases (proportionately) as the particle size increases. With the assumption that this contribution scales with the surface area of the interface, a $1/R$ dependence is expected and indeed this is roughly what is found when plotting (not shown) the $CH_2\cdots O$ VdW energy. The values in italics in Table 3 underneath the $CH_2\cdots O$ VdW energies give the surface energies in J m^{-2}. These are very similar irrespective of the size of the particle and the volume fraction of silica.

3.1.2. Density and Volume Fraction. Although not shown in the tables, the mean cell lengths and cell angles for the relaxed systems indicated that all the boxes were close to being cubic. For any particular system, cell lengths were the same to within ~1 Å and all cell angles were in the range from 88° to 92°. Such deviations from a perfectly cubic shape are not unusual for systems of this size. In general, the near cubic shape confirms the good isotropy of the systems.

It is interesting to note that the average density of the composite systems, at both the lower and higher volume fractions of silica, increases slightly with increasing particle size. This can be largely explained by the way in which the nanoparticles are constructed. Although the composite preparation technique used gives a mass of polymer strictly proportional to R_n^3, only the initial number of Si and O atoms in a particle is proportional to R_n^3; the subsequent use of the iterative algorithm to create the surface structure eliminates Si and O atoms in a way which is proportional to the surface area, i.e., R_n^2. The result is seen clearly in the behavior of the mass fraction of silica (Table 3) that marginally increases with particle size as the surface term becomes less important compared to the volume. For the same reasons, the relative proportion of O and Si changes with particle size and a plot of the O:Si ratio (not shown) for the three particle sizes can be fitted very well to the function $2 + \lambda/R_n$ with a value of the constant $\lambda \approx 5.1$. Another inevitable consequence of this surface area to volume ratio effect is that the true volume fractions of silica are not exactly constant for the systems nominally at the same "low" (~4.5%) and "high" (~27%) volume fractions of silica. Although the exact volume fractions are not so important for the purpose of this paper, they are required input for the subsequent micromechanical calculations. It is useful then to try and determine the volume occupied by the different components both in anticipa-

Table 5. Values of Various Quantities Related to the Volume Occupied by the Different Components as Obtained from the Analysis of the Composite Systems at 100 K Using a Random Probe Insertion Technique (See Text for Details)[a]

		R15L	R30L	R60L	R30H	R60H
	R_s/Å	13.00 ± 0.03	28.11 ± 0.07	58.05 ± 0.05	28.07 ± 0.01	58.05 ± 0.01
	ΔR/Å	2.7 ± 0.1	2.7 ± 0.2	2.6 ± 0.3	2.74 ± 0.04	2.63 ± 0.04
$R_{sc} = R_s + \Delta R/2$	R_{sc}/Å	14.36 ± 0.05	29.4 ± 0.2	59.4 ± 0.1	29.44 ± 0.02	59.36 ± 0.02
	% V_{sc}	3.98 ± 0.01	4.28 ± 0.02	4.37 ± 0.01	26.80 ± 0.02	27.01 ± 0.01
	ρ_{silica}/kg m^{-3}	2436 ± 8	2417 ± 11	2457 ± 5	2420 ± 2	2461.8 ± 0.4
	ρ_{matrix}/kg m^{-3}	779.7 ± 0.2	778.8 ± 0.2	778.0 ± 0.1	797.9 ± 0.3	787.1 ± 0.2
$R_{sc} = R_s + \Delta R/3$	R_{sc}/Å	13.91 ± 0.04	29.0 ± 0.1	58.9 ± 0.1	28.98 ± 0.02	58.92 ± 0.02
	% V_{sc}	3.62 ± 0.01	4.09 ± 0.02	4.28 ± 0.01	25.57 ± 0.02	26.42 ± 0.01
	ρ_{silica}/kg m^{-3}	2677 ± 8	2530 ± 11	2515 ± 5	2536 ± 2	2516.2 ± 0.7
	ρ_{matrix}/kg m^{-3}	776.7 ± 0.2	777.3 ± 0.2	777.2 ± 0.1	784.8 ± 0.2	780.8 ± 0.1

[a] R_s is the effective radius of the silica particle, ΔR is the interfacial thickness, and R_{sc} is the corrected radius of the silica particle. Two different approximations to R_{sc} are given in the table. % V_{sc} is the volume fraction obtained from R_{sc} expressed as a percentage. Densities given are based on the known mass of each component and the average volume as partitioned according to the volume fraction calculation.

tion of associated work and for the principle reason here of explaining the increase in density with particle size. This is not a trivial task in the case of the small particles, as in here, where surface roughness is significant with respect to their size. Ultimately, as particle size increases, all methods should converge as the spherical approximation becomes better and better. Here, we have used a fairly crude but simple random probe insertion technique in that a combination of different analyses gives reasonably reliable values for the volumes occupied by the silica and the polymer.

To begin the analysis, it is first assumed that the entire volume of the MD box, V_{box}, can be divided into three distinct parts: the volume accessible to the centers of the Si and O atoms in the silica, V_s, plus the volume accessible to the centers of the CH_2 sites of the polymer, V_p, plus the volume inaccessible, V_i, to the centers of either, i.e., the interface. Thus

$$V_{box} = V_s + V_p + V_i \tag{7}$$

To access the different components of the volume, the stored configurations of the systems are analyzed using a technique originally developed to determine the void space, i.e., the volume accessible to a probe of a certain size, R_{probe}. The method involves trial insertions of a virtual probe at random places in the MD box. If none of the atoms in the box fall within a distance of R_{probe} plus the radius of the atom, then the probe is considered "accepted". The probe accessible volume is then just the fraction of accepted insertions multiplied by V_{box} in the limit of a doing a large number of trials; in practice, 10 trials per Å^3 are sufficient to obtain good convergence within reasonable computational times. Here, a radius of 1.5 Å was used for all atoms as well as the virtual probe as the first peak in the O$\cdot\cdot\cdot$$CH_2$ radial distribution function is at about 3 Å. By use of the technique in the way it was designed on the composite systems, the probe accessible volume will be equivalent to the sum of void space in the polymer, V_{vp}, plus the void space in the silica, V_{vs}; for any given configuration, the polymer or silica atoms do not occupy all of V_p and V_s. However, if during the analysis all silica atoms are invisible to the probe then the probe accessible volume found is equal to $V_s + V_{vp}$. Alternatively, if CH_2 atoms are turned off we obtain $V_p + V_{vs}$. Nominally then, from the three different probe insertion tests, we have only three equations but four unknowns. To resolve the problem, the approximation is made so that the proportion of void space in the silica particle is the same as that found in the bulk silica model. This latter value is quite small, 0.066% for the probe size of 1.5 Å. With the approximation that $V_{vs} = 0.00066V_s$, it is thus possible to determine V_{vp}, V_s, and V_p and hence obtain V_i from the known box volume and eq 7.

This method was then used to obtain these contributions to the volumes in the five composite systems at 100 K by averaging over the configurations stored during the final 1500 ps of the relaxation simulations. For the three low volume fraction systems, log−log plots (not shown) of these volume contributions against R_n show that the increase in V_p is dominated by a term proportional to R_n^3, although closer inspection reveals a term in R_n^2 also. The interfacial volume V_i is clearly largely dependent on R_n^2, as would be expected for an interface of roughly constant width. However, the volume of silica varies in a manner intermediate between R_n^3 and R_n^2. Indeed, as for the mass of silica, V_s fits well to the form $\alpha R_n^3 - \beta R_n^2$, with α and β being constants. To a good approximation, the preparation procedure thus gives rise to a situation where the total volume and total mass have a dependence of the form $\alpha R_n^3 - \beta R_n^2$. Fitting the total mass and the total volume independently to this form and then dividing the respective fits gives the prediction for the density shown in Figure 3. Apart from the deviation at the lowest value of R_n, the fit is reasonably good and the best-fit coefficients predict a limiting density of ∼854 kg m^{-3}.

To obtain approximations for the volume fractions of silica and polymer, the problem that still remains is how to partition the interfacial volume between the silica and the polymer. To do this, an effective radius of silica, R_s, is first calculated assuming that the particle is completely spherical, $R_s = (3V_s/4\pi)^{1/3}$. The interfacial thickness, ΔR, is then obtained in a similar manner by assuming that the interface volume is distributed evenly over the surface of a sphere, $\Delta R = (3(V_s + V_i)/4\pi)^{1/3} - R_s$. A corrected radius for silica, R_{sc}, can then be obtained by assuming that a certain inner fraction of the interfacial thickness equally is effectively occupied by the silica. In Table 5, two results are shown for comparison for estimations using $R_{sc} = R_s + \Delta R/2$ and $R_{sc} = R_s + \Delta R/3$. As partitioning of the interfacial thickness equally does not take into account the different sizes of the atoms, the second estimate using $^1/_3$ probably reflects a better approximation, the first peak in the radial distribution function for the $CH_2\cdots CH_2$ interactions being at about 4 Å.

The behavior with R_n of the volume fraction of silica obtained using $R_{sc} = R_s + \Delta R/3$ is shown in Figure 4 for the three composite systems at the lower volume fraction of silica at 100 K. The dotted line shown in the figure is simply a result of fitting the corrected volume of silica to the form $\alpha R_n^3 - \beta R_n^2$ and then dividing this by the best fit for the total volume to same form. The numerical fit here agrees quite well with the actual data even at low R_n. The best-fit coefficients imply a limiting volume fraction of silica at large R_n of ∼4.47%, a value close to our original target value of 4.5%.

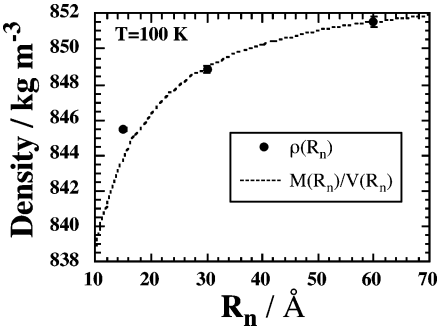

Figure 3. The mean densities of the three composite systems at the lower volume fraction of silica at 100 K. The dotted line is the result of dividing independent fits of the total mass, $M(R_n)$, and the total volume, $V(R_n)$, to the form $\alpha R_n^3 - \beta R_n^2$.

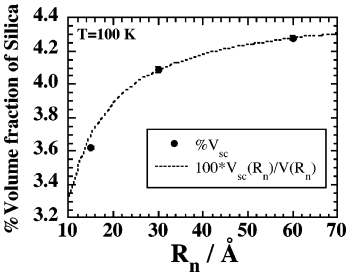

Figure 4. The volume fraction of silica obtained from the virtual probe insertion technique using a corrected radius defined as $R_{sc} = R_s + \Delta R/3$ for the three low silica volume fraction composite systems at 100 K. The dotted line gives a prediction of the behavior of the volume fraction based on independent fits of the corrected volume of silica, $V_{sc}(R_n)$, and the total volume, $V(R_n)$, to the form $\alpha R_n^3 - \beta R_n^2$.

3.1.3. Glass Transition. Values of the T_g, as evaluated from fits of the specific volume to the form of eq 5, for the different nanocomposites and the pure matrix are given in Table 4. The sizable error bars on T_g evaluated in this way do not permit us to say whether the presence of the inclusions induces a significant change in the glass transition temperature.

Another common experimental method of determining T_g is the differential scanning calorimetry (DSC) that essentially probes changes in the enthalpy of a system. For this reason, plots of the enthalpy ($H = U + PV$) against temperature were also generated for the cooling runs and the data fitted to the form of eq 5. In these systems, the enthalpy generally shows more important changes in the slope than the volume alone and the resulting glass transition temperatures, also shown in Table 2, are thus subject to somewhat smaller errors. However, the values obtained for the pure matrix and the nanocomposite systems are within 6 K of each other and hence within errors. A resolution of the internal energy into its component parts reveals that the bonding and bending contributions change linearly with temperature, as might be expected from their harmonic nature. Only the torsion energy and the Van der Waals energy exhibit nonlinearity. Again, plotting these terms as a function of temperature and fitting to the form of eq 5 allow two other estimates of T_g to be made, also shown in Table 2. The values for the torsion energy are in good agreement with those for the enthalpy as the torsion energy is by far the dominant of the two nonlinear terms; typically the torsion energy changes are at least 8 times higher than those of the VdW energy in the range from 450 down to 0 K. In effect, the fits to the VdW energy with temperature have to be considered as being fairly unreliable given the relatively feeble changes in slope.

The last indicator of the glass transition that has been investigated is the variation of the fraction of *trans* conformers with temperature. In all systems, the *trans* fraction increases almost linearly in the range from 450 to 300 K before gradually tending to a plateau value, generally attained in the region of 200 K. Fits of this behavior to eq 5 are not as good given the broad range of the transition, so the values of the T_g obtained from this route, shown in Table 2, have to be treated with caution. Nevertheless, it can be seen for the pure matrix all estimates of the glass transition temperature are in good agreement. For the composite systems, leaving aside the unreliable estimates from the VdW energy, there is again agreement within the estimated error bars.

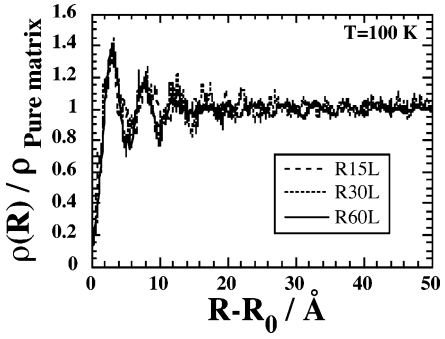

Figure 5. The normalized radial mass density of the polymer as a function of the distance from the interface, $R - R_0$, for the three nanocomposites at the lower volume fraction at 100 K. A resolution of 0.1 Å was used for the accumulation of these histograms.

Experimentally a decrease in T_g of about 25 K has been observed in alumina−PMMA composites, albeit with particle sizes considerably larger, 390 Å,[41] and this effect was attributed to an increase in molecular mobility. Interestingly, the decrease could be avoided by precoating the alumina to render it more compatible with the matrix. It is tempting to attribute this again to the interphase and thus to expect the effect to accentuate with particle size, assuming an interphase of fixed thickness. Our data does not seem to suggest that this is the case.

A complementary analysis has been performed on the R60L nanocomposite system during the heating and cooling cycle in order to see if local variations of the T_g exist. This system contains enough atoms to permit the reliable calculation of certain properties of the polymer matrix in concentric shells (see next section) around the center-of-mass (COM) of the nanoparticle. However, the changes in slopes of the density vs *T* and *%trans* vs *T* curves in the shells were very similar to the global values and thus no radial dependence of T_g could be detected.

3.2. Molecular Structure. In this section, the changes induced in the structure of the polymer matrix by the inclusion of the silica nanoparticles are presented. The nanoparticle being highly spherical the spatial variation of the polymer structure and mobility have been analyzed simply with respect to the distance, *R*, from the center-of-mass of the silica nanoparticle to a CH_2 site. The histograms presented have been accumulated with respect to *R* and by averaging over the last 1500 ps of the simulation.

3.2.1. Mass Distribution. In Figure 5, the mass density of polymer, $\rho(R)$, as a function of the distance from the interface, $R - R_0$, is presented for the composite systems at the low volume fraction at 100 K. *R* is the distance from the center-of-mass of the silica nanoparticle to a CH_2 site, and R_0 is defined from the position of the first peak in $\rho(R)$ as $R_0 = R_1 - 3$, with $\rho(R_1)$ being the first maximum and 3 Å being the distance over which $\rho(R)$ rises from very small values up to the first peak. This definition of the position of the interface is complicated by the roughness of the surface of the silica particle. The position of the first peak in $\rho(R)$ is a position which is statistically well

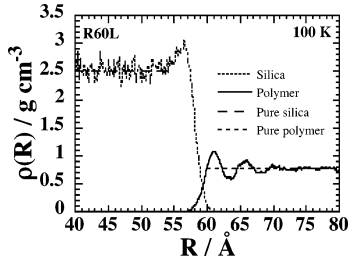

Figure 6. The radial mass densities of the silica and the polymer in the $R_n = 60$ Å composite at low volume fraction at 100 K. The two distributions overlap by about 5 Å in the interfacial region. Horizontal lines are there just to indicate the limiting bulk values and are taken from the simulations of the pure systems.

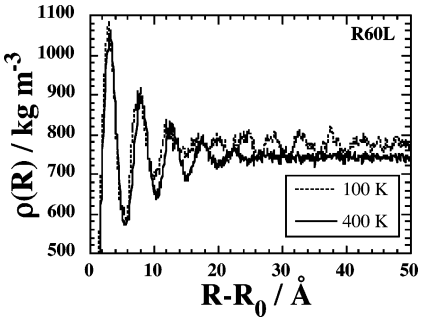

Figure 7. The radial mass density of the polymer as a function of the distance from the interface, $R - R_0$, for the R60L composite at 100 and 400 K.

defined compared to, for example, the minimum value observed for R for the CH_2 sites, which depends very much on the surface roughness and has very low statistical weight. The problem of surface roughness can be seen in Figure 6 that shows the radial mass densities of the silica and the polymer in the case of the R60L composite. The two distributions overlap in a zone of width ~5 Å.

Figure 5 shows that, in a range of at least 20 Å from the interface, successive oscillations occur with a decaying amplitude until the density of the pure matrix is attained. Such a structuring has been observed before for chains of this generic type in the presence of plain walls and nanofillers.[1,6,8,42] Within the statistical precision of the data, the structure is independent of the inclusion size implying a constant thickness of the interphase. Furthermore, the results for $\rho(R)$ from the R30H and R60H systems (not shown) are very similar also suggesting that the interphase thickness does not depend on the volume fraction when the particles are perfectly dispersed.

In order to see if the interphase thickness is dependent on temperature, all five composite systems and the 30-chain pure matrix have also been relaxed at the higher temperature of 400 K. The starting configurations for these studies have been extracted from the heating part of the T_g determination tests. The different systems were then relaxed for 2 ns under NPT conditions at 400 K and 5000 bar. Averages were again obtained from the last 1.5 ns of the simulations. As an example, the results for the radial density for the R60L system at 400 K are compared to those obtained at 100 K in Figure 7. The first three peaks in the $\rho(R)$ superimpose quite well although there is a slight broadening of the peaks at the higher temperature, which leads to a gradual dephasage, and the limiting values are clearly different due to the expected volume dilation. Indeed, the limiting value of $\rho(R)$ at the higher temperature is in good agreement with the average density of 742.8 ± 0.1 kg m^{-3} obtained for the pure 30-chain matrix relaxed at 400 K. The higher temperature also leads to a significant smoothing of the

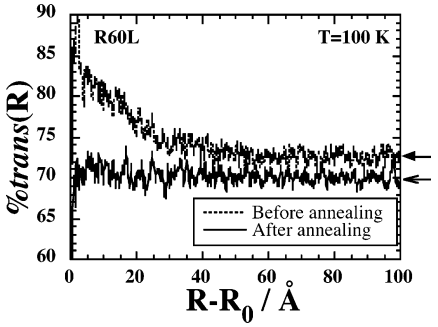

Figure 8. The radial dependence of the mean percentage of *trans* conformers in the R60L system at 100 K. The full line gives the average distribution over the last 1500 ps of the simulation. The dashed line gives the average distribution prior to the heat treatment. The arrow to the right marks the mean % trans in the pure matrices.

tail of the distribution compared to the 100 K result, and distinct fourth and fifth peaks can now be seen. At 100 K, it is hard to tell from $\rho(R)$ precisely where the structuring stops due to the statistical noise. It is thus difficult to say whether the interphase thickness increases or decreases with temperature although the similarity in the first three peaks suggest that the temperature can only have a marginal effect and that, to a good approximation, a constant thickness can be assumed.

3.2.2. Conformer Distribution. The average percentages of backbone −C−C−C−C− *trans* conformers were given for each simulation at 100 K in Table 2. A −C−C−C−C− torsion angle is defined to be *trans* if it is within ±60° of the minimum in the *trans* well of the torsion angle potential. Unlike our previous simulations,[25] the inclusion of the nanoparticle appears to lead here to *decreases* in the *% trans* of up to 2.5%. Previously,[25] the opposite trend of an increase in the fraction of *trans* conformers was attributed to the construction step, where the cavity was introduced into the matrix, and the subsequent inability for the chains to relax on the time scale of the simulation. This led to a noticeable gradient in the *% trans* with respect to the distance from the surface, see Figure 2 of ref 25. To investigate this further, the radial dependence of the *% trans* has again been determined. For each −C−C−C−C− torsion angle, the center-of-mass of the four atoms involved is calculated, and the distance, R, from it to the center-of-mass of the silica nanoparticle is determined. Histograms, of width 0.1 Å, are then accumulated containing the total number of angles and the number of these that are in the *trans* state. Examples of the resulting *% trans*(R) distributions are shown in Figure 8 in the case of the R60L system both before (dashed line) and after (full line) the annealing step. The comparison reveals clearly that the heating to 1000 K under NVT conditions, and subsequent rapid cooling, has a significant effect not only on the R dependence but also on the average value. Before annealing, the distribution is qualitatively similar to that found previously[25] with a *% trans* elevated close to the interface which returns to the pure matrix value over a distance of 40−50 Å; the filled arrow to the right of the figure indicates the average value found for the pure matrix of 72.6% following the initial relaxation, i.e., before the second heat treatment. After annealing the composite, the R dependence has not only largely vanished but also the limiting large R value has been changed. This latter effect is due to a subtle difference in the way that the initial annealing step was performed in the pure matrices as compared to the composites or to the second annealing step for the pure matrices. In the case of the pure matrices, the first annealing was performed at the initial density of ~632 kg m^{-3} used to construct the cells and *not* a density corresponding to an

overpressure of 5000 bar at 100 K; only afterward were the matrices relaxed under NPT conditions. For the composites, and the pure matrices for the second annealing, the fixed-volume annealing was done *after* a prerelaxation under NPT conditions at 5000 bar at 100 K. In short, the densities of the polymer matrices were not the same during the annealing cycles. In the composites, and the pure polymers during the second annealing, the higher density of the polymer leads to a freezing out of conformational changes, during the rapid quench from 1000 K, at an earlier time (higher temperature) and we thus obtain *% trans* marginally lower than the pure matrices after the first heat treatment, or the unannealed composites, as seen for all the finally relaxed pure matrices (Table 2) and composite systems at 100 K (Table 3). It can be seen though from Figure 8 that the limiting large R value of the *% trans* in the R60L composite does tend toward the average value for the 640-chain matrix following second heat treatment (open arrow).

Clearly, the conformational degrees of freedom are very sensitive to the thermal history. It should be noted that the much slower cooling rates used in the simulations to obtain T_g lead to significantly higher percentages of *trans* conformers, in excess of 80%. Indeed during the initial heating cycle of the T_g determination runs, the *% trans* actually first *increases* with temperature, up to ~300 K, before decreasing.

Despite the clear structuring in the density, the *% trans* shows very little structure after the annealing phase. Clearly, the local stretching of chains that takes place when the initial cavity is made is largely relaxed out by the heat treatment. There is some residual effect as the *% trans* is slightly higher in the interphase region, which is enough to give average values of 0.4−0.8% higher than the corresponding pure matrices (see Tables 2 and 3) in the low volume fraction systems. The residual effect is more important in the R30H and R60H systems, where the averages are ~2% higher than the corresponding matrices. The distributions though remain relatively featureless and resemble very much the one for R60L "after annealing" shown in Figure 8.

The effect of temperature is also marginal. Distributions (not shown) of the *% trans(R)* obtained from the simulations at 400 K are shifted upward, for the reasons mentioned concerning the thermal history, and are smoother but otherwise have the same pattern with a modest enhancement in the interphase region and a gradual return to the average value for the pure matrix (75.2 ± 0.1 for the 30-chain system).

3.2.3. Alignment Distribution. The local orientation of chain segments induced by the nanoparticle has also been characterized as a function of R in the same way as described previously.[25] Each consecutive triplet of the CH_2 sites on the chain $\{i,j,k\}$ are considered, and the angle θ is defined to be as that between the vector from the center-of-mass of the nanoparticle to particle j and the vector between particles i and k, i.e., that between the outwardly pointing vector normal to the interface and the local axis of the polymer chain. This angle can then be used to define second-order Legendre polynomial function

$$P_2(\cos\theta) = \frac{3}{2} <\cos^2\theta> - \frac{1}{2} \qquad (8)$$

which can then be accumulated as a histogram in R. $P_2(\cos\theta)$ is plotted as a function of R in Figure 9 for the three nanocomposites at the lower volume fraction at 100 K. Unlike the *% trans*, the local orientation of chains around the inclusion is clearly structured although the values are in general somewhat reduced compared to our previous study,[25] this being also a consequence of the annealing step. Otherwise, the results are very similar with chains being aligned perpendicular to the outward pointing normal to the interface, i.e., tangential to the interface, at low values of $R - R_0$. There then follow a number of oscillations of decreasing amplitude in the alignment with troughs of tangential alignment corresponding to the peaks in radial density. It is noticeable from the results for the R60L system, where the statistics are much better, that the orientation decreases only very gradually with R once the oscillations have died away and does not reach the random value of zero over the limited range displayed in Figure 9. For this reason, the same data has been replotted in Figure 10 out to a larger range of R. It seems from this plot that a random orientation is only attained beyond a range of 100 Å from the interface, i.e., considerably further out than could be seen in either the radial density or the *% trans*. It should be pointed out that to obtain data out to the range shown in Figure 10 it is necessary to go beyond the usual "limit" defined by the largest inscribable sphere in the MD box. For the R60L system, the half-box length is ~136 Å, so the value of $R - R_0$ corresponding to the radius of the largest inscribable sphere is 136 − 58 = 78 Å. Nevertheless, despite the truncation of the averaging sphere, there are as many angles in a shell of width 0.1 Å at $R - R_0 \sim 130$ Å as there are at $R - R_0 \sim 20$ Å. Beyond ~130 Å though the statistics become rapidly very poor as we start to probe the "corners" of the MD box, i.e., $R - R_0 > 136\sqrt{2} - 58 \approx 134$ Å.

Also plotted in Figure 10 is the data for the same R60L system at the higher temperature of 400 K. There is clearly no significant effect on the thickness of the interphase as probed by the $P_2(\cos\theta)$ function. Although not shown, data for the systems at higher volume fraction show no significant differences from those presented for the R60L in the obviously much more restricted range of $R - R_0$.

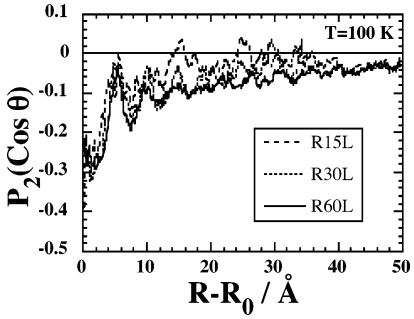

Figure 9. The mean values of $P_2(\cos\theta)$ plotted as a function of the distance from the interface for the three low volume fraction composite systems at 100 K. (See text for definition of θ.)

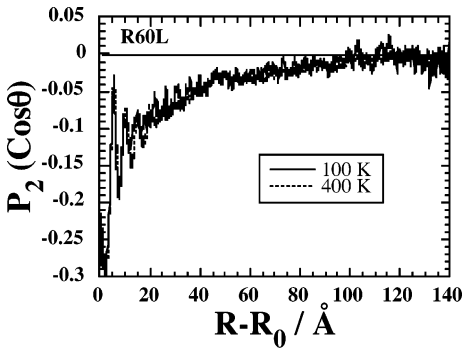

Figure 10. The mean values of $P_2(\cos\theta)$ plotted as a function of the distance from the interface for the R60L composite systems at 100 and 400 K. Note that the range of $R - R_0$ is larger than that shown in Figure 9.

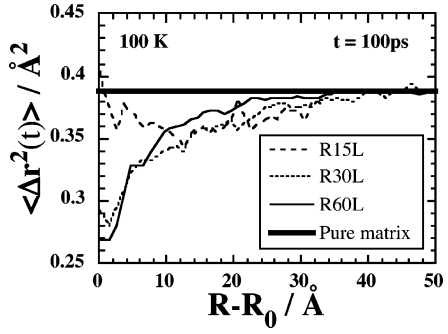

Figure 11. The mean-square displacements of the polymer at a time interval of 100 ps as a function of the distance from the interface, $R - R_0$, for the three nanocomposites at the lower volume fraction at 100 K. A resolution of 1 Å was used for the accumulation of these histograms. The thick horizontal line is the MSD of the CH_2 sites in the 640-chain pure matrix system at a time interval of 100 ps.

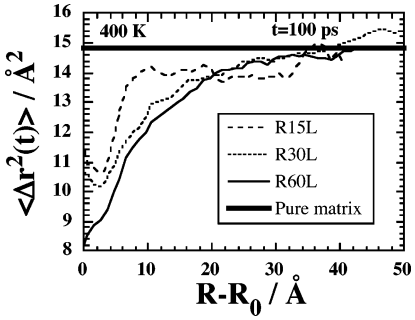

Figure 12. Same as Figure 11 at 400 K. The thick horizontal line is the MSD of the CH_2 sites in the 30-chain pure matrix system at a time interval of 100 ps.

3.3. Molecular Mobility. In this section the changes induced in the dynamics of the polymer matrix by the inclusion of the silica nanoparticles are presented. As in the previous section, variations have been analyzed with respect to R and by averaging over the last 1500 ps of the simulations.

3.3.1. Mean-Square Displacements. The square displacement of a particular atom, i, at a time interval t with respect to a certain time origin, t_0, is calculated in the following way from the trajectory generated in the course of an NPT simulation

$$\Delta r_i^2(t) = (\mathbf{r}_i(t + t_0) - \mathbf{h}(t + t_0)\mathbf{h}^{-1}(t_0)\mathbf{r}_i(t_0))^2 \qquad (9)$$

where $\mathbf{h}$ represents the 3×3 matrix of basis vectors, $\{\mathbf{a}, \mathbf{b}, \mathbf{c}\}$, describing the shape and size of the MD cell. As $\mathbf{h}$ varies with time, the operation in eq 9 avoids including displacements arising simply from changes in the shape and size of the MD box. As explained in detail previously, the R-dependent variation of the mean-square displacements, MSD, of the CH_2 sites can be calculated to see if there is any evidence for the influence of the nanoparticle on local mobility. The results obtained for a time interval of 100 ps at 100 K for the three composite systems at the lower volume fraction are shown in Figure 11. Averages have been taken over all possible time origins in the last 1500 ps of the simulations. It can be seen immediately that the MSDs are very small in these systems that are well below the glass transition. The MSDs here simply represent the degree of local fluctuations in position and cannot be related to any diffusive motion.

In the R60L and R30L systems, there is, in agreement with our previous results,[1] a clear reduction in the MSDs close to the interface with a gradual rise back to the pure matrix value on moving further away from the interface; plots (not shown) of the MSDs for the R30H and R60H higher volume fraction

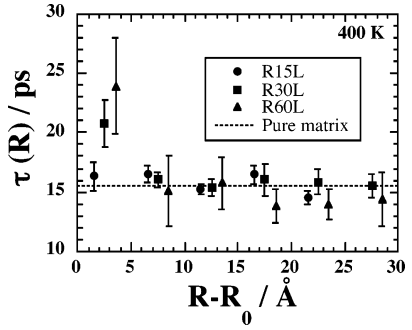

Figure 13. The radial dependence of the relaxation time for the $C_{TT}(t)$ function (eq 13). All values are for averages taken in 5 Å shells around the nanoparticle COM. The points have been offset slightly for the three systems along the x axis for clarity. The dotted line simply indicates the value obtained for the 30-chain pure polymer system at 400 K.

systems show a very similar trend. The R15L system, however, shows a quite different behavior. Although the gradual decrease in MSD in the region from 15 to 40 Å is similar to that in the other systems, this trend is reversed as the interface is approached. In the R15L system, there are fewer particles in the concentric shells close to the interface, so this may be a statistical problem. Tests on the pure matrix systems, using the center-of-mass of the entire system as a pseudo-origin for the radial density functions, reveal that statistical problems start to occur for R less than ~20 Å, i.e., the values of the MSD for $R - R_0 < 10$ Å should be treated with caution in the case of the $R_n = 15$ Å system.

The same functions have also been studied at the higher temperature of 400 K and the results for the lower volume fraction systems are plotted in Figure 12. In this case, the MSDs are considerably larger, for the same time interval of 100 ps, and are well beyond that expected of librations within a local well. All systems now show a clear reduction in the translational mobility close to the interface. Again, results (not shown) for the higher volume fraction confirm this result. We note that a reduced polymer mobility in the vicinity of the inclusion has also been reported in NMR studies of composites.[4,5]

3.3.2. Torsional Relaxation. To evaluate the possible effects of the presence of the nanoparticle on the *trans*−*gauche* interconversion dynamics of the polymer backbone torsional modes, relaxation functions of the form

$$R_{TT}(t) = \langle H_T\{\alpha_i(t_0)\}\, H_T\{\alpha_i(t_0 + t)\}\rangle \qquad (10)$$

were computed. In eq 10, $\alpha_i(t)$ is the torsion angle of the ith C−C−C−C torsion at time t and the function $H_T\{\alpha_i(t)\}$ is the characteristic function of the *trans* conformation. $H_T\{\alpha_i(t)\} = 1$ if $-60° \le \alpha_i(t) \le 60°$ or 0 otherwise. $R_{TT}(t)$ effectively measures the fraction of C−C−C−C torsion angles that were in a state *trans* at some arbitrary origin in time, t_0, and that are in the *trans* state at a time interval, t, later. Its use in studying isomerization dynamics has been detailed elsewhere.[43] Here, we use it to probe the possible effect of the nanoparticle on the torsional mobility of the polymer. The normalized correlation function, $C_{TT}(t)$, is defined as

$$C_{TT}(t) = \frac{R_{TT}(t) - \langle X_T\rangle^2}{\langle X_T\rangle - \langle X_T\rangle^2} \qquad (11)$$

where $\langle X_T\rangle = R_{TT}(0)$ is the mean *trans* fraction. As has been done in the past,[1,26] we resolve this function into concentric shells, of 5 Å thickness, around the COM of the nanoparticle.

This assignment was based on the position of the center-of-mass of the four atoms involved in the torsion at the time origin, t_0. Although this means that at some later time an angle may belong to a different shell, it does avoid the bias that would result from selecting only angles that remain in a particular shell. In any case, diffusion is relatively low so this should not be a problem.

At 100 K, the degree of decorrelation in $C_{TT}(t)$ is very small in the time scale of the simulations undertaken, as might be expected for chains well below the glass transition. For this reason, the same functions were also evaluated at the higher temperature of 400 K. The resulting $C_{TT}(t)$ (not shown) decayed relatively quickly, compared to those at 100 K, and were found to fit well to the stretched exponential Kohlrausch−Williams−Watts (KWW) functional form :

$$C_{TT}(t) = \exp\left(-\left(\frac{t}{\alpha}\right)^{\beta}\right) \tag{12}$$

Best-fit values for α and β were obtained using nonlinear least-squares regression over the range from 0 to 200 ps. The corresponding relaxation times were then obtained from the analytic time integral of the stretched exponential:

$$\tau = \int_0^{\infty} \exp\left(-\left(\frac{t}{\alpha}\right)^{\beta}\right) \mathrm{d}t = \frac{\alpha}{\beta}\int_0^{\infty} s^{(1/\beta)-1}\exp(-s)\,\mathrm{d}s = \frac{\alpha}{\beta}\Gamma\left(\frac{1}{\beta}\right) \tag{13}$$

where the gamma function was estimated to high precision using a standard numerical technique.[44] The results for the radial dependence of τ are plotted in Figure 13 for the lower volume fraction systems. There is some indication that the decreased translational mobility near the interface increases the relaxation time associated with the establishment of *trans−gauche* equilibrium in the R60L and R30L systems, but otherwise most of the τ values are very close to that obtained for the pure 30-chain matrix system relaxed at 400 K (shown as a dotted line in Figure 13). Again, this finding is largely in agreement with previous studies.[1,26]

Conclusion

From the radial dependence of the structural and dynamic properties shown above concerning the low volume fraction composites, it is clear that, for nanocomposites constructed in the way described here, the interphase thickness seems to depend somewhat on the property examined. Whether this is a real effect or is simply a perceived result due to the different levels of statistical noise remains to be determined by further more exhaustive studies. However, it seems fairly clear that, for a given property, the interface thickness is relatively insensitive to the size of the filler particle. The results for the higher volume fraction confirm this finding and also show that there is also little sensitivity of the interface thickness to the volume fraction either. Tests at a much higher temperature do not reveal any drastic changes in this scenario, so, to a good approximation, it is reasonable to assume that the interphase thickness is independent of the particle size. Thus, for a fixed volume fraction of filler, a decreasing inclusion size leads to a possible increase of the influence of the interphase of disturbed matrix on the overall behavior of the nanocomposite. This is the main conclusion of this current work as it underpins the basis on which comparisons will be made with micromechanical modeling of the same type of nanocomposite systems. The confrontation between the results obtained for the mechanical properties of the atomistically detailed nanocomposites constructed here and the predictions of such a continuum mechanics approach will be the subject of a forthcoming article.

Acknowledgment. The IDRIS (Orsay, France) and the CINES (Montpellier, France) computer centres are acknowledged for the provision of supercomputer time. The French Ministry of Education and Technological Research is thanked for providing the doctoral grant for V.M. and also partially financing the project under the ACI 2001 programme "*SURFACES, INTERFACES ET CONCEPTION DE NOUVEAUX MATERIAUX*". We acknowledge many fruitful discussions held with Professors Eveline Hervé and André Zaoui (LMS, Ecole Polytechnique−CNRS, France) during the course of this work.

References and Notes

(1) Brown, D.; Mélé, P.; Marceau, S.; Albérola, N. *Macromolecules* **2003**, *36* (4), 1395−1406.
(2) Dutta, N. K.; Roy Choudhury, N.; Haidar, B.; Vidal, A.; Donnet, J. B. *Polymer* **1994**, *35* (20), 4293−4299.
(3) Mansencal, R.; Haidar, B.; Vidal, A.; Delmotte, L.; Chezeau, J.-M. *Polym. Int.* **2001**, *50* (4), 387−394.
(4) Berriot, J.; Lequeux, F.; Monnerie, L.; Montes, H.; Long, D.; Sotta, P. *J. Non-Cryst. Solids* **2002**, *307-310*, 719−724.
(5) Berriot, J.; Martin, F.; Montes, H.; Monnerie, L.; Sotta, P. *Polymer* **2003**, *44* (5), 1437−1447.
(6) Vacatello, M. *Macromolecules* **2001**, *34* (6), 1946−1952.
(7) Vacatello, M. *Macromol. Theory Simul.* **2002**, *11* (5), 501−512.
(8) Starr, F. W.; Schrøder, T. B.; Glotzer, S. C. *Phys. Rev. E* **2001**, *64* (2), 021802.
(9) Starr, F. W.; Schrøder, T. B.; Glotzer, S. C. *Macromolecules* **2002**, *35* (11), 4481−4492.
(10) Kasemagi, H.; Klintenberg, M.; Aabloo, A.; Thomas, J.-O. *J. Mater. Chem.* **2001**, *11* (12), 3191−3196.
(11) Odegard, G. M.; Clancy, T. C.; Gates, T. S. *Polymer* **2005**, *46* (2), 553−562.
(12) Chevalier, Y.; Hidalgo, M.; Cavaillé, J.-Y.; Cabane, B. *Macromolecules* **1999**, *32*, 7887−7896.
(13) Hajji, P.; David, L.; Gerard, J. F.; Pascault, J. P.; Vigier, G. *J. Polym. Sci., Part B : Polym. Phys.* **1999**, *37* (22), 3172−3187.
(14) Marceau, S. Architecture Multiéchelle et Propriétés Mécaniques de Nanocomposites. Ph.D. Thesis, University of Savoie, Bourget-du-Lac, 2003. Available at http://www.lmops.univ-savoie.fr/people/smarceau/.
(15) Griebel, M. Hamaekers, J. *Comput. Methods Appl. Mech. Eng.* **2004**, *193*, 1773−1788.
(16) de Gennes, P.-G. *Scaling Concepts in Polymer Physics*; Cornell University Press: Ithaca, New York, 1979; p 323.
(17) Tsuneyuki, S. *Mol. Eng.* **1996**, *6* (1 & 2), 157.
(18) Fincham, D. *Inf. Q. Comput. Simul. Condens. Phases* **1993**, *38*, 17−24.
(19) van Beest, B. W. H.; Kramer, G. J.; van Santen, R. A. *Phys. Rev. Lett.* **1990**, *64* (16), 1955−1958.
(20) Vollmayr, K.; Kob, W.; Binder, K. *Phys. Rev. B* **1996**, *54* (22), 15808−15827.
(21) Brown, D. *The gmq User Manual*, Version 3, 1999. Web site. http://www.lmops.univ-savoie.fr/brown/gmq.html.
(22) Berendsen, H. J. C.; Postma, J. P. M.; van Gunsteren, W. F.; DiNola, A.; Haak, J. R. *J. Chem. Phys.* **1984**, *81*, 3684−3690.
(23) Brown, D.; Clarke, J. H. R. *Comput. Phys. Commun.* **1991**, *62*, 360−369.
(24) Brown, D.; Neyertz, S. *Mol. Phys.* **1995**, *84* (3), 577−595.
(25) Brown, D.; Marceau, S.; Mélé, P.; Albérola, N. D. *Molecular dynamics studies of model silica-polymer nanocomposite systems*, Eurofillers 2003, University of Alicante, Spain, Sept 8−11, 2003; pp 209−212.
(26) Barbier, D.; Brown, D.; Grillet, A.-C.; Neyertz, S. *Macromolecules* **2004**, *37* (12), 4695−4710.
(27) Zhuravlev, L. T. *Colloids Surf., A* **2000**, *173*, 1−38.
(28) Brodka, A.; Zerda, T. W. *J. Chem. Phys.* **1996**, *104* (16), 6319−26.
(29) Gallo, P.; Rovere, M.; Ricci, M. A.; Hartnig, C.; Spohr, E. *Philos. Mag., B* **1999**, *79* (11−12), 1923−30.
(30) Song Hi, L.; Rossky, P. J. *J. Chem. Phys.* **1994**, *100* (4), 3334−45.
(31) Brown, D.; Clarke, J. H. R. *Macromolecules* **1991**, *24* (8), 2075−2082.
(32) Brown, D.; Clarke, J. H. R.; Okuda, M.; Yamazaki, T. *J. Chem. Phys.* **1994**, *100* (2), 1684−1692.
(33) Brown, D.; Clarke, J. H. R.; Okuda, M.; Yamazaki, T. *J. Chem. Phys.* **1994**, *100* (8), 6011−6018.

(34) Brown, D.; Clarke, J. H. R.; Okuda, M.; Yamazaki, T. *J. Chem. Phys.* **1996**, *104* (5), 2078−2082.
(35) Neyertz, S.; Brown, D. *J. Chem. Phys.* **2001**, *115*, 708.
(36) Neyertz, S. *Soft Mater.* **2007**, *4* (1), 15−83.
(37) McKechnie, J. I.; Haward, R. N.; Brown, D.; Clarke, J. H. R. *Macromolecules* **1993**, *26*, 198−202.
(38) Humphrey, W.; Dalke, A.; Schulten, K. J. *Mol. Graphics* **1996**, *14* (1), 33−38.
(39) Brown, D.; Minoux, H.; Maigret, B. *Comput. Phys. Commun.* **1997**, *103* (2,3), 170−186.
(40) Brown, D.; Maigret, B. *Speedup* **1999**, *12* (2), 33−40.
(41) Ash, B. J.; Schadler, L. S.; Siegel, R. W. *Mater. Lett.* **2002**, *55* (1,2), 83−87.
(42) Bitsanis, I.; Hadziioannou, G. *J. Chem. Phys.* **1990**, *92* (6), 3827−3847.
(43) Brown, D.; Clarke, J. H. R. *J. Chem. Phys.* **1990**, *92* (5), 3062−3073.
(44) Lanczos, C. *SIAM J. Numer. Anal.* **1964**, *B1*, 86−96.

MA701940J